

# Field Evolution of the Fulde-Ferrell-Larkin-Ovchinnikov State in a Superconductor with Strong Pauli Effects

Kenta M. SUZUKI, Yasumasa TSUTSUMI, Noriyuki NAKAI<sup>1</sup>, Masanori ICHIOKA, and Kazushige MACHIDA

*Department of Physics, Okayama University, Okayama 700-8530, Japan*

<sup>1</sup>*Nanoscience and Nanotechnology Research Center (N2RC), Osaka Prefecture University, 1-2 Gakuen-cho, Sakai 599-8570, Japan*

The Fulde-Ferrell-Larkin-Ovchinnikov (FFLO) phase in the vortex lattice state is quantitatively studied using the self-consistent Eilenberger theory in three-dimensional (3D) space. We estimate free energy to determine the FFLO phase diagram in the  $H$ - $T$  plane and stable FFLO wave number in the isotropic system with the 3D Fermi sphere and  $s$ -wave pairing. To facilitate the experimental identification of the FFLO state, we investigate the field evolution of NMR spectra and flux line lattice form factors obtained in neutron scattering in the FFLO vortex states. Possible applications of our results to experimental data on CeCoIn<sub>5</sub> are mentioned.

**KEYWORDS:** heavy-fermion superconductors, Fulde-Ferrell-Larkin-Ovchinnikov state, vortex state, quasi-classical Eilenberger theory

There has been much attention focused on discovering and hunting exotic superconducting states. Among them, in the singlet pairing category, the Fulde-Ferrell-Larkin-Ovchinnikov (FFLO) state has been one of the most elusive examples since its theoretical prediction in 1964.<sup>1,2)</sup> In the FFLO states, the superconducting order parameter exhibits a spatial modulation.<sup>3)</sup> The population imbalance is brought about either by the application of an external field in the charged electron case through the Zeeman effect or by the preparation of up and down species in cold neutral atom gases.<sup>4-6)</sup> Under an applied field, the FFLO state is expected to be the one most likely to emerge in the low-temperature ( $T$ ) high-field ( $H$ ) region. So far there is no direct evidence to prove the existence of the FFLO state in either the charged or neutral system. Thus the FFLO state still remains elusive. In the charged system, the orbital depairing effect due to electron diamagnetic motion in a magnetic field cannot be ignored since it may affect the stability of the FFLO state.

On the other hand, there has been no microscopic calculation of the field evolution of the FFLO state that fully takes account of the orbital depairing effect, namely, the vortex effect beyond the Ginzburg-Landau (GL) framework valid near the upper critical field ( $H_{c2}$ ).<sup>7)</sup> In particular, the Larkin-Ovchinnikov (LO) state with a periodically modulated amplitude of the order parameter is highly difficult to describe owing to the solitonic spatial variation with infinitely many higher harmonics in general.<sup>8)</sup> In CeCoIn<sub>5</sub>, it is suggested that the LO state is realized rather than the Fulde-Ferrell (FF) state in which only the phase is modulated in the order parameter.<sup>3)</sup> In the LO state, there are two possible modulation directions with respect to the applied magnetic field: longitudinal and transverse. In this letter, we consider the longitudinal LO state in the vortex lattice. Hereafter, the longitudinal LO vortex state will simply be called the FFLO state. To investigate the stability of the FFLO state against a magnetic field, we solve the microscopic Eilenberger equations self-consistently in the three-dimensional (3D) space composed of the in-plane vortex lattice and the longitudinal FFLO modulation, taking into account the orbital and Pauli-paramagnetic depairings on

an equal footing.

Furthermore, to provide fundamental theoretical information on physical quantities in the FFLO state, we examine the effects of the FFLO modulation on the nuclear magnetic resonance (NMR)<sup>9-12)</sup> and flux line lattice (FLL) form factors obtained in a small-angle neutron scattering (SANS)<sup>13,14)</sup> experiment. It will become apparent that these two methods can provide direct and crucial evidence of the FFLO state, among the variety of other experiments.<sup>3,15)</sup> We will discuss anomalous behaviors in the corresponding experimental data on the heavy Fermion superconductor CeCoIn<sub>5</sub>, the high-field and low-temperature superconducting phase of which is regarded to be a realization of the FFLO state. Thus the main purpose of this letter is to demonstrate the NMR spectrum and FLL form factors through the theoretical study.

Our basic strategy is to provide  $H$ -dependent properties of the FFLO states for the 3D Fermi sphere and  $s$ -wave pairing. The corresponding 3D calculation for the FF state<sup>16)</sup> and the full self-consistent analytical theory for a quasi-1D case<sup>8)</sup> have been performed previously in the Pauli limiting case without vortices. Here, we extend those calculations to take account of vortex effects. Before discussing the anomalous behavior of the FFLO states in CeCoIn<sub>5</sub>, it is necessary to clarify the quantitative properties of the FFLO state in a typical example of the 3D Fermi sphere.

We calculate the spatial structure of the vortex lattice state using the quasi-classical Eilenberger theory in the clean limit valid for  $k_F \xi \gg 1$  ( $k_F$  is the Fermi wave number and  $\xi$  is the superconducting coherence length).<sup>17,18)</sup> The Pauli paramagnetic effects are included through the Zeeman term  $\mu_B \mathbf{B}(\mathbf{r})$ , where  $\mathbf{B}(\mathbf{r})$  is the flux density of an internal field and  $\mu_B$  is a renormalized Bohr magneton. The quasi-classical Green's functions  $g(\omega_n + i\mu_B, \mathbf{k}, \mathbf{r})$ ,  $f(\omega_n + i\mu_B, \mathbf{k}, \mathbf{r})$ , and  $f^\dagger(\omega_n + i\mu_B, \mathbf{k}, \mathbf{r})$  are calculated in the vortex lattice state by the Eilenberger equations<sup>19,20)</sup>

$$\begin{aligned} \{\omega_n + i\mu_B + \tilde{\mathbf{v}} \cdot (\nabla + i\mathbf{A})\} f &= \Delta g, \\ \{\omega_n + i\mu_B - \tilde{\mathbf{v}} \cdot (\nabla - i\mathbf{A})\} f^\dagger &= \Delta^* g, \end{aligned} \quad (1)$$

where  $g = (1 - f f^\dagger)^{1/2}$ ,  $\text{Reg} > 0$ ,  $\tilde{\mathbf{v}} = \mathbf{v}/v_{F0}$ , and the Pauli

parameter  $\mu = \mu_B B_0 / \pi k_B T_c$ .  $\mathbf{k}$  is the relative momentum of the Cooper pair, and  $\mathbf{r}$  is the center-of-mass coordinate of the pair.  $\mathbf{v}$  is the Fermi velocity and  $v_{F0} = \langle v^2 \rangle_{\mathbf{k}}^{1/2}$  where  $\langle \dots \rangle_{\mathbf{k}}$  indicates the Fermi surface average. We assume a magnetic field is applied to the  $z$ -axis. The Eilenberger units of  $R_0$  for lengths and  $B_0$  for a magnetic field are used.<sup>19,20</sup> The order parameter  $\Delta$  and the Matsubara frequency  $\omega_n$  are normalized in units of  $\pi k_B T_c$ .

For self-consistent conditions, the order parameter is calculated by

$$\Delta(\mathbf{r}) = g_0 N_0 T \sum_{0 < \omega_n \leq \omega_{\text{cut}}} \langle f + f^{*+} \rangle_{\mathbf{k}} \quad (2)$$

with  $(g_0 N_0)^{-1} = \ln T + 2T \sum_{0 < \omega_n \leq \omega_{\text{cut}}} \omega_n^{-1}$ . We use  $\omega_{\text{cut}} = 20 k_B T_c$ .  $\mathbf{B} = \nabla \times \mathbf{A}$  is self-consistently determined by

$$\nabla \times (\nabla \times \mathbf{A}) = \nabla \times \mathbf{M}_{\text{para}}(\mathbf{r}) - \frac{2T}{\kappa^2} \sum_{0 < \omega_n} \langle \tilde{v} \text{Im } g \rangle_{\mathbf{k}}, \quad (3)$$

where we consider both the diamagnetic contribution of supercurrent in the last term and the contribution of the paramagnetic moment  $\mathbf{M}_{\text{para}}(\mathbf{r}) = (0, 0, M_{\text{para}}(\mathbf{r}))$  with

$$M_{\text{para}}(\mathbf{r}) = M_0 \left( \frac{B(\mathbf{r})}{H} - \frac{2T}{\mu H} \sum_{0 < \omega_n} \langle \text{Im } g \rangle_{\mathbf{k}} \right). \quad (4)$$

The normal state paramagnetic moment  $M_0 = (\mu/\kappa)^2 H$ ,  $\kappa = B_0 / \pi k_B T_c \sqrt{8\pi N_0}$  and  $N_0$  is the density of states at the Fermi energy in the normal state. We set the GL parameter  $\kappa$  to be 102. We solve eq. (1) and eqs. (2)-(4) alternately, and obtain self-consistent solutions, as in previous works,<sup>19,20</sup> under a given unit cell of the triangular vortex lattice. For the FFLO state,  $\Delta(\mathbf{r})$  has a periodic oscillation with the period  $L$  in addition to the vortex lattice structure. As the unit cell size of the vortex lattice is determined by  $H = \langle \mathbf{B} \rangle_{\mathbf{r}}$ , we can estimate the  $H$ -dependence of the FFLO state in our calculation of the vortex lattice. Throughout this paper we use  $\mu = 5$  as a representative case of the strong Pauli paramagnetic effect.

The Gibbs free energies are calculated from self-consistent solutions using eq. (9) in ref. 21 for the FFLO state with various FFLO wavelengths  $L$ . We compare them to identify the most stable state under a given  $H$  and  $T$ . Figure 1(a) exhibits the resulting successive changes at  $T/T_c = 0.1$ . It is seen that, starting from  $H = H_{c2}$  where the FFLO state with the shortest wavelength  $L = 17$  is stabilized,  $L$  becomes longer as  $H$  decreases. Eventually the free energy of the FFLO state becomes comparable to that of the conventional Abrikosov state, where the FFLO modulation along the field direction is absent. The envelope of the free energies of the FFLO state approaches that of the Abrikosov state, such that the two curves seem to merge tangentially, namely, at the meeting point, tangents of the two curves coincide with each other. While our calculations are for discretized  $L$ , even these results suggest (1) a second-order-like transition between the FFLO state and the Abrikosov vortex state<sup>7)</sup> and (2) the continuous  $L$  change of the FFLO state as a function of  $H$ , which are similar to the results of previous analytic FFLO theory.<sup>8)</sup>

In Fig. 1(b), we show the phase diagram in the  $H$ - $T$  plane. This is obtained by repeating the FFLO calculations as a function of  $H$  at different temperatures,  $T/T_c = 0.1, 0.15, 0.2$ , and  $0.25$ .  $H_{LO}$  is the transition field from the Abrikosov vortex

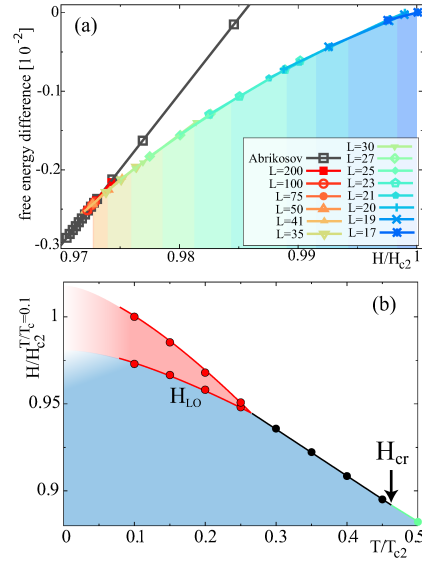


Fig. 1. (Color online) (a) Free energy differences  $F$  from the normal state for the FFLO state with different wave numbers  $L$  and the Abrikosov state, as a function of  $H$ .  $T = 0.1T_c$ . In the normal state,  $F = 0$ . (b) Phase diagram for the FFLO state in the  $H$ - $T$  plane for the 3D Fermi sphere and the  $s$ -wave pairing.  $\mu = 5$ .  $H_{c2}$  is the first order at  $H > H_{cr}$ . Lines are guides for the eye.

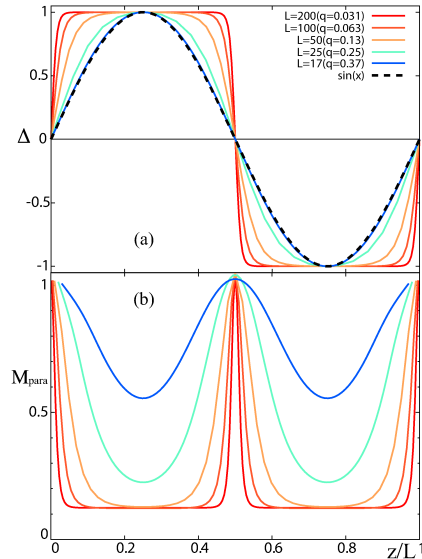


Fig. 2. (Color online) Spatial variations of (a) the order parameter  $\Delta(\mathbf{r})$  and (b) the paramagnetic moment  $M_{\text{para}}(\mathbf{r})$  for several values of  $L$  along the field direction outside of vortices. These are normalized by its length and maximum values.  $T/T_c = 0.1$  and  $\mu = 5$ .

state to the FFLO state and the transition at  $H_{c2}$  to the normal phase is the first order above  $H_{cr}$ . The FFLO region in the  $H$ - $T$  plane is given by  $H_{LO}/H_{c2} = 0.973$  for the present  $\mu = 5$  at  $T/T_c = 0.1$ . The value of  $H_{LO}/H_{c2}$  depends on the  $\mu$  value, namely,  $H_{LO}/H_{c2} = 0.991$  for  $\mu = 2$  at  $T/T_c = 0.1$ . Even in this strong paramagnetic case of  $\mu = 5$ , the FFLO phase appears only near  $H_{c2}$ , and  $H_{LO}$  increases on lowering  $T$  in this typical example of an isotropic Fermi sphere.

Figure 2 displays normalized waveforms of (a) the order parameter  $\Delta(\mathbf{r})$  and (b) the paramagnetic moment  $M_{\text{para}}(\mathbf{r})$  in

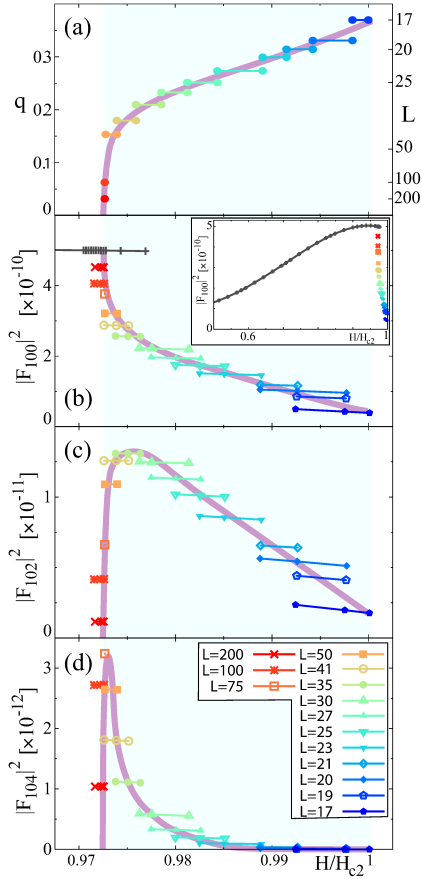


Fig. 3. (Color online) Field evolutions of various quantities at  $T/T_c = 0.1$  and  $\mu = 5$ . (a) FFLO wave number  $q = 2\pi/L$ . (b) Form factor  $|F_{100}|^2$ . Inset shows the overall variation. (c) Form factor  $|F_{102}|^2$ . (d) Form factor  $|F_{104}|^2$ .

the FFLO state along the field direction outside of vortices. It is seen that a simple sinusoidal modulation waveform continuously deforms into an anti-phase kink form, or solitonic waveform as  $H$  approaches the  $H_{LO}$  line where  $L$  diverges. In other words, near the  $H_{LO}$  boundary, the sign change or  $\pi$  phase shift of the order parameter occurs sharply, meaning that the excess electrons and  $M_{\text{para}}(\mathbf{r})$  are confined in a narrow spatial region along the kink position.

The FFLO nodal kink forms a sheet of paramagnetic moments perpendicular to the field. On the other hand, along the vortex lines, enhanced  $M_{\text{para}}(\mathbf{r})$  at the vortex core is decreased at the intersection with FFLO kink plane (see Fig. 2 in ref. 19 and Fig. 1 in ref. 22). There, the zero-energy peak states of quasiparticles are absent, because of the  $2\pi$  phase shift of the order parameter, coming from the kink and from the vortex. The paramagnetic moment becomes strongly confined to the kink position as  $H$  approaches  $H_{LO}$  from above. As will be seen later, these three-dimensional FFLO spatial structures can be probed by SANS experiments or NMR experiments.

As shown in Fig. 3(a), the FFLO wave number  $q = 2\pi/L$  of the stable FFLO state continuously varies with  $H$ . Starting with  $q = 0$  at  $H = H_{LO}$ ,  $q$  increases sharply. Hence the antiphase solitonic waveform quickly changes into a sinusoidal one on increasing  $H$  (see also Fig. 2). This behavior is similar to that seen in the exact solution (see Fig. 9 in ref. 8), implying that the FFLO physics along the parallel direction exemplified here is common and universal.

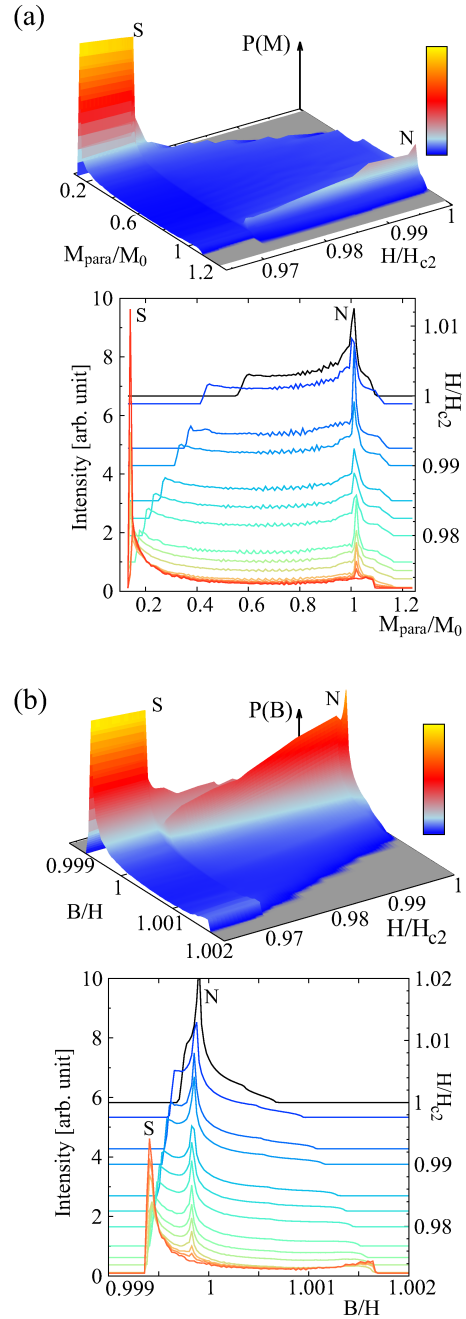


Fig. 4. (Color online) NMR spectra in the FFLO state: (a) paramagnetic moment distribution  $P(M)$  (b) and internal field distribution  $P(B)$ .  $\mu = 5$  and  $T/T_c = 0.1$ . Upper panels show  $H$ -evolution of spectra in stereographic view. Lower panels show spectra at some values of  $H$ . Horizontal baselines for each spectrum are shifted by  $H/H_{c2}$ , which is indicated on the right axis.

The FLL form factor is an important quantity that can be directly measured in a SANS experiment. The form factors  $F_{hkl}$  are Fourier components of an internal field  $\mathbf{B}(\mathbf{r})$  in our calculation.<sup>19)</sup> The fundamental Bragg spots  $F_{100}$  for the vortex lattice are shown in Fig. 3(b) as a function of  $H$ . The spot  $|F_{100}|^2$  increases in the Abrikosov state, because  $M_{\text{para}}(\mathbf{r})$  accumulates at the vortex core to increase  $B(\mathbf{r})$  locally, as seen in the inset of Fig. 3(b). This feature has already been shown theoretically<sup>20)</sup> and observed in various paramagnetically enhanced superconductors, such as  $\text{TmNi}_2\text{B}_2\text{C}$ <sup>23)</sup> and

CeCoIn<sub>5</sub>.<sup>14</sup> As shown in Fig. 3(b), the intensity of  $|F_{100}|^2$  suddenly decreases upon entering the FFLO phase and continues to drop quickly, almost exponentially. (Note the  $T = 50$  mK data in Fig. 1 of ref. 24). This is because  $M_{\text{para}}(\mathbf{r})$  is not enhanced at the vortex core on the FFLO nodal plane (see Fig. 5(b) in ref. 19). This contribution decreases  $|F_{100}|^2$ , which is the average along the  $z$ -axis.

In addition to the usual Bragg spots  $F_{100}$  associated with the vortex lattice, the observation of extra spots  $F_{10n}$  ( $n = 2, 4, \dots$ ) is crucial to prove the existence of the FFLO phase. In Fig. 3(c), we show  $|F_{102}|^2$ , which is the new superspot associated with the FFLO modulation along the field direction. It rises quickly at  $H = H_{\text{LO}}$ . After attaining a maximum in the middle of the FFLO phase, it slowly decreases towards  $H_{\text{c2}}$ . Thus the best chance to observe it is in the middle field region inside the FFLO phase. The relative intensity  $|F_{102}|^2/|F_{100}|^2 = 1/10 \sim 1/20$ . Therefore it is quite possible to detect it because  $|F_{100}|^2$  is enhanced by the Pauli effect even near  $H_{\text{c2}}$ . The higher order spot  $|F_{104}|^2$  is also shown in Fig. 3(d). It takes a maximum just near  $H_{\text{LO}}$ . Since the magnitude of  $|F_{104}|^2$  is further reduced and is one order of magnitude smaller than  $|F_{102}|^2$ , it might be difficult to detect it.

The NMR spectrum is also crucial to identify the FFLO state. By choosing probed nuclei that have different hyperfine coupling constants, we can effectively pick up the selective field distributions.<sup>19</sup> When the hyperfine coupling is sufficiently strong, the paramagnetic distribution  $M_{\text{para}}(\mathbf{r})$  is probed in NMR experiments. In contrast, in the weak coupling case, the magnetic induction  $B(\mathbf{r})$  in the whole system is detected by NMR. In the mixed state of ordinary superconductors, it yields the so-called Redfield pattern.

Here, we examine the field evolution of the NMR spectra for both strong and weak hyperfine coupling cases. For the former (latter), we evaluate the distribution  $P(M)$  [ $P(B)$ ] using the stable FFLO state at each field. These are given by

$$P(M) = \int (M - M_{\text{para}}(\mathbf{r})) d\mathbf{r}, \quad P(B) = \int (B - B(\mathbf{r})) d\mathbf{r}, \quad (5)$$

i.e., volume counting for each  $M$  and  $B$ . Figure 4 shows the spectral evolutions of these distributions for two cases. In Fig. 4(a),  $P(M)$  is displayed. Since in the Abrikosov state the paramagnetic moment is confined exclusively to the vortex cores, a single main peak appears at the saddle point (S) position in the NMR spectrum. In the FFLO phase,  $M_{\text{para}}(\mathbf{r})$ , which comes from excess electrons, accumulates at the normal state (N) position. The peak at the N-position becomes dominant towards  $H_{\text{c2}}$ , because an increasing excess of unpaired quasiparticles appear at the FFLO nodal sheets. It is noted that near  $H_{\text{LO}}$ , two peaks appear simultaneously in the NMR spectrum. This double peak structure was observed in the In(2) site of the NMR spectrum by Kumagai *et al.*<sup>12</sup> for CeCoIn<sub>5</sub>. The appearance of the double peaks at S- and N-positions is unambiguous evidence of the FFLO state.

It is also important to observe the characteristic change of  $P(B)$  for the weak hyperfine case, exemplified by In(1) in CeCoIn<sub>5</sub>. Here, rather unexpectedly, the double peak structure can be seen in Fig. 4(b) near  $H_{\text{LO}}$ , beyond which the N peak dominates the spectrum. The N-position is near the S-position in  $P(B)$ , compared with  $P(M)$ . In the lower field of the Abrikosov state, the usual Redfield pattern is reproduced,

as seen from Fig. 4(b).

We touch upon the recent NMR experiment on CeCoIn<sub>5</sub>.<sup>12</sup> The observed double peak structure of In(2a) for  $H \parallel c$  and  $H \parallel ab$  is markedly similar to our result in Fig. 4(a) (see the spectral evolution in Fig. 2 of ref. 12). The proposed phase diagram of FFLO for  $H \parallel c$  is also similar to our Fig. 1(b) where  $H_{\text{LO}}/H_{\text{c2}} \sim 0.975$  for  $\mu = 5$  compared with  $H_{\text{LO}}/H_{\text{c2}} = 4.7T/4.95T \sim 0.95$  at zero temperature for  $H \parallel c$ .<sup>11</sup> As mentioned previously, the value of  $H_{\text{LO}}/H_{\text{c2}}$  depends on  $\mu$ , but the shape of the FFLO phase diagram is hardly changed by the value of  $\mu$ . For  $H \parallel ab$ , the proposed phase diagram is modified because of the presence of the existing SDW.<sup>25</sup>

We also calculated the FFLO structure in  $d$ -wave pairing or the quasi-two-dimensional Fermi surface when a magnetic field is applied to the  $z$ -axis. These situations do not qualitatively change the results shown in Figs. 2-4. Careful estimation of the free energy to determine the stable  $L$  remains for future work.

In conclusion, we quantitatively explored the field evolution of the FFLO state for typical examples of a Fermi sphere and  $s$ -wave pairing, by self-consistently solving the microscopic Eilenberger equations in the 3D space of the vortex lattice and the FFLO modulation along the field direction. To facilitate the identification of the FFLO state through experiments, we estimate the NMR spectrum and FLL form factors as a function of the magnetic field in the FFLO vortex states.

The authors are grateful for insightful discussions with M. Kenzelmann, S. Gerber, J. S. White, J. L. Gavilano, T. Sakakibara, E. M. Forgan, K. Kumagai, R. Ikeda, Y. Matsuda, and M. R. Eskildsen.

- 1) P. Fulde and R. A. Ferrell: Phys. Rev. **135** (1964) A550.
- 2) A. I. Larkin and Y. N. Ovchinnikov: Zh. Eksp. Teor. Fiz. **47** (1964) 1136. [translation: Sov. Phys. JETP **20** (1965) 762].
- 3) See for review, Y. Matsuda and H. Shimahara: J. Phys. Soc. Jpn. **76** (2007) 051005.
- 4) T. Mizushima, K. Machida, and M. Ichioka: Phys. Rev. Lett. **94** (2005) 060404.
- 5) K. Machida, T. Mizushima, and M. Ichioka: Phys. Rev. Lett. **97** (2006) 120407.
- 6) M. W. Zwierlein, A. Schirotzek, C. H. Schunck, and W. Ketterle: Science **311** (2006) 492; M. W. Zwierlein, C. H. Schunck, A. Schirotzek, and W. Ketterle: Nature (London) **442** (2006) 54; G. B. Partridge, W. Li, R. I. Kamar, Y. Liao, and R. G. Hulet: Science **311** (2006) 503.
- 7) R. Ikeda and H. Adachi: Phys. Rev. B **69** (2004) 212506 and references therein.
- 8) K. Machida and H. Nakanishi: Phys. Rev. B **30** (1984) 122.
- 9) B.-L. Young, R. R. Urbano, N. J. Curro, J. D. Thompson, J. L. Sarrao, A. B. Vorontsov, and M. J. Graf: Phys. Rev. Lett. **98** (2007) 036402.
- 10) G. Koutroulakis, V. F. Mitrović, M. Horvatić, C. Berthier, G. Lapertot, and J. Flouquet: Phys. Rev. Lett. **101** (2008) 047004.
- 11) K. Kumagai, M. Saitoh, T. Oyaizu, Y. Furukawa, S. Takashima, M. No-hara, H. Takagi, and Y. Matsuda: Phys. Rev. Lett. **97** (2006) 227002.
- 12) K. Kumagai, H. Shishido, T. Shibauchi, and Y. Matsuda: Phys. Rev. Lett. **106** (2011) 137004.
- 13) M. Kenzelmann, Th. Strässle, C. Niedermayer, M. Sgrist, B. Padmanabhan, M. Zolliker, A. D. Bianchi, R. Movshovich, E. D. Bauer, J. L. Sarrao, and J. D. Thompson: Science **321** (2008) 1652; M. Kenzelmann, S. Gerber, N. Egetenmeyer, J. L. Gavilano, Th. Strässle, A. D. Bianchi, E. Ressouche, R. Movshovich, E. D. Bauer, J. L. Sarrao, and J. D. Thompson: Phys. Rev. Lett. **104** (2010) 127001.
- 14) A. D. Bianchi, M. Kenzelmann, L. DeBeer-Schmitt, J. S. White, E. M. Forgan, J. Mesot, M. Zolliker, J. Kohlbrecher, R. Movshovich, E. D. Bauer, J. L. Sarrao, Z. Fisk, C. Petrović, and M. R. Eskildsen: Science **319** (2008) 177.



- 15) A. Bianchi, R. Movshovich, C. Capan, P. G. Pagliuso, and J. L. Sarrao: Phys. Rev. Lett. **91** (2003) 187004.
- 16) S. Takada and T. Izuyama: Prog. Theor. Phys. **41** (1969) 635.
- 17) M. Ichioka, N. Hayashi, and K. Machida: Phys. Rev. B **55** (1997) 6565.
- 18) M. Ichioka, A. Hasegawa, and K. Machida: Phys. Rev. B **59** (1999) 184; M. Ichioka, A. Hasegawa, and K. Machida: Phys. Rev. B **59** (1999) 8902.
- 19) M. Ichioka, H. Adachi, T. Mizushima, and K. Machida: Phys. Rev. B **76** (2007) 014503.
- 20) M. Ichioka and K. Machida: Phys. Rev. B **76** (2007) 064502.
- 21) M. Hiragi, K. M. Suzuki, M. Ichioka, and K. Machida: J. Phys. Soc. Jpn. **79** (2010) 094709.
- 22) T. Mizushima, K. Machida, and M. Ichioka: Phys. Rev. Lett. **95** (2005) 117003.
- 23) L. DeBeer-Schmitt, M. R. Eskildsen, M. Ichioka, K. Machida, N. Jenkins, C. D. Dewhurst, A. B. Abrahamsen, S. L. Bud'ko, and P. C. Canfield: Phys. Rev. Lett. **99** (2007) 167001.
- 24) J. S. White, P. Das, M. R. Eskildsen, L. DeBeer-Schmitt, E. M. Forgan, A. D. Bianchi, M. Kenzelmann, M. Zolliker, S. Gerber, J. L. Gavilano, J. Mesot, R. Movshovich, E. D. Bauer, J. L. Sarrao and C. Petrovic: New J. Phys. **12** (2010) 023026.
- 25) K. M. Suzuki, M. Ichioka, and K. Machida: Phys. Rev. B **83** (2011) 140503(R).